Environment Protection Engineering

Vol. 51 2025 No. 2

DOI: 10.37190/epe250207

YANG GUOHAO [1], HE ZHIMING [1]
SUN JIAWEI [2], GUO HAO [2], ZHANG KAI [1]

MECHANISM OF THE EFFECT OF MODIFIED TiO_2 ON THE STRENGTH OF GOLD TAILINGS-BASED NO-FIRE BRICKS SAMPLES

Brick-making from gold tailings is one of the common utilization methods, however, this method usually requires pressurized sintering. This study investigates the effect of modified TiO_2 on the strength of gold tailings-based no-fire bricks under ambient temperature and pressure conditions. Gold tailings, river sand, and gravel were used as raw materials, with cement-epoxy resin serving as the composite binder and modified TiO_2 acting as the reinforcing agent. The surface of TiO_2 was modified by silane coupling agent KH-560 and polyethyleneimine (PEI), and the effect of modified TiO_2 on the performance and characterization of gold tailings-based no-fire bricks was investigated. The results show that 25% KH-560 silane coupling agent and 75% polyethyleneimine (PEI) modify TiO_2 best. The optimal compressive strength of 79.6 MPa was achieved in gold tailings-based no-fire bricks with 2% modified TiO_2 addition. Microscopic morphology and chemical analysis confirmed that the modified TiO_2 significantly enhanced the structural integrity of gold tailings-based no-fire bricks.

1. INTRODUCTION

A large number of tailings ponds have caused serious damage to the ecological environment. Under the requirement of green mine construction, the approval of tailing pond construction in China has become more and more strict [1]. According to China's tailings data statistics in 2018, the gold tailings emissions in the mining industry are about 216 million t, accounting for 17.84% of the national tailings emissions, and the utilization rate of gold tailings in the country is only 36.9%, which shows that a large number of gold tailings are in an idle state. In the past decades, a lot of research has

[1]Inner Mongolia University of Science and Technology, Baotou, Inner Mongolia, China.

[2]Inner Mongolia Autonomous Region Nuclear and Radiation Monitoring Centre, Baotou, Inner Mongolia, China, corresponding author Z. Kai, email address: 2021023147@stu.imust.edu.cn

been carried out on the comprehensive utilization of tailings, such as the recovery of valuable elements, the production of building materials, and the use of concrete aggregates [2]. However, all these utilization methods can only handle a small portion of the tailings, and the vast majority of gold tailings are still stored in tailings ponds. As a result, serious environmental problems are caused long after the closure of the mining site, so academics are now encouraged to develop the best waste recycling and disposal solutions to promote environmental and economic sustainability [3, 4]. Currently, for tailings treatment and its resource utilization, biological treatment, and solidification/stabilization (S/S) are widely applied [5–8] such as the preparation of sintered bricks from gold tailings [9], gold tailings for concrete [10], ceramics from gold tailings [11]. However, the vast majority of brick-making processes at this stage require strength to be provided by sintering and pressurization. At room temperature and pressure, the fineness modulus of most gold tailings is much smaller than the national specification for mud and stone dust content [12]. Therefore, at the present stage, gold tailings brick-making not only has a substantial increase in the demand for cementitious materials but also has poorer curing and stabilization effectiveness and lower compressive strength compared to other tailings. Therefore, this paper achieves the enhancement of the curing performance of gold tailings-based no-fire bricks by using modified TiO_2 as a reinforcing agent.

Nano TiO_2 is a nanomaterial with high mechanical properties, electromagnetic wave shielding and absorption properties, antimicrobial properties, strong redox properties, and acid and alkali corrosion resistance. Its particles are usually spherical or ellipsoidal and exist in powder, sol-gel, and suspension forms [13]. Because of its quantum tunneling effect, quantum size effect, and surface effect, it is widely used in construction materials to enhance the mechanical properties of the curing body and durability [14–16]. At the present stage, on the one hand, nanomaterials are thought to be able to improve the durability and mechanical characteristics of cured bodies. At this stage, on the one hand, it is thought that the internal structure and interfacial interactions of nano TiO_2 materials play a major role in determining their mechanical characteristics. The gelling material crystallizes at the interface due to the nucleation effect played by the nano TiO_2 particles. In the form of a non-covalent bonding combination, a more favorable curing structure is formed by altering the interfacial adhesive force [17, 18]. On the other hand, it is believed that the fine nano-TiO_2 particles will affect the mixing characteristics of concrete and the filling effect in the curing process, which will improve the void structure of the cured body, and ultimately improve the macroscopic mechanical properties of the cured matrix [19, 20]. Therefore, the effect of nano TiO_2 on the gelling material mainly exists in the physical effects such as interfacial interactions and fine void filling. Nano TiO_2 has a good enhancement effect on the curing of materials, but there are some shortcomings [21]: Because nano TiO_2 has high surface energy, it is very easy to agglomerate in the gelling material, and it is not easy to be dispersed uniformly in the gelling material due to its high cohesive force, making it difficult for the performance of nano TiO_2 to achieve the expected effect. Therefore, the dispersion problem of nano

TiO_2 is a central challenge for researchers. The surface of nano TiO_2 contains almost only hydroxyl groups, which makes it difficult to undergo chemical cross-linking, and if it can be chemically cross-linking with the gelling material, this will further improve the strength of the composite material. Therefore, the chemical cross-linking of nano TiO_2 is another difficult problem faced by researchers.

This study modified TiO_2 surfaces to improve their dispersion in gold tailings-based no-fire bricks. The effect of physical interactions and chemical cross-linking enhanced the compressive strength of the bricks. The findings provide a theoretical basis for future practical applications of TiO_2 in gold tailings-based no-fire brick production. Therefore, the objectives of this study were to (1) investigate a modified TiO_2 that enhances the properties of gold tailings-based no-fire bricks, (2) investigate the effect of modified TiO_2 on the compressive strength of gold tailings-based no-fire bricks, and (3) explore the possible curing/stabilization (S/S) mechanism of modified TiO_2.

2. MATERIALS AND METHODS

2.1. MATERIALS

The studied gold tailings (Inner Mongolia Autonomous Region) were dried at 105 °C and ground to powder form for this study. The chemical composition of the gold tailings was carried out by X-ray fluorescence spectrometry (XRF). The crystal structure of the gold tailings was analyzed and determined by X-ray diffraction (XRD). The fineness modulus of the gold tailings was determined by sieving. The loss on ignition (LOI) of the material at 800 °C was analyzed by thermogravimetry, and the cyanide (CN) leaching concentration of the tailings was tested by silver nitrate titration. The chemical composition, physical composition, LOI, and CN-leaching concentration of the tailings are shown in Fig. 1 and Table 1.

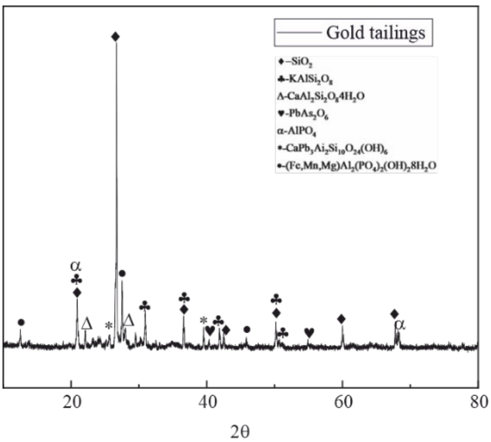

Fig. 1. XRD of gold tailings

Table 1

Chemical composition and physical properties of gold tailings

Oxide	Content [%]	Oxide/Properties	Content [%]
SiO_2	62.24	TiO_2	0.68
Al_2O_3	13.89	P_2O_5	0.11
Fe_2O_3	7.84	loss on ignition	2.83
K_2O	5.87	fineness modulus	0.53
CaO	5.20	CN^- content	3.75 mg/dm^3
SO_3	1.14		

The cement is based on an ordinary silicate cement P-O42.5, as shown in Table 2.

Table 2

Chemical composition of cement

Oxide	CaO	SiO_2	Al_2O_3	MgO	SO_3	TiO_2	Fe_2O_3	K_2O
Content, %	33.33	31.02	18.56	13.07	2.23	0.89	0.24	0.20

Epoxy resin is mainly composed of epoxy resin A and B glue with the composition ratio of 4:1 (Table 3).

Table 3

Epoxy resins

<table>
<tr><td rowspan="2">Resin A adhesive, E-51</td><td>Epoxy value, g/mol</td><td>Viscosity, mPa·s</td><td colspan="2">Colour (Pt-Co)</td><td>Hydrolysis of chlorine, %</td></tr>
<tr><td>184–195</td><td>10 000–16 000</td><td colspan="2">≤40</td><td>≤0.5</td></tr>
<tr><td rowspan="2">Resin B hardener, 593</td><td>Appearance</td><td colspan="2">Viscosity, mPa·s</td><td colspan="2">Amine value (mg KOH/OH)</td></tr>
<tr><td>clear liquid</td><td colspan="2">100±50</td><td colspan="2">500–600</td></tr>
</table>

Other materials used in the experiments are presented in Table 4.

Table 4

Other materials used

Material	Specification	Factory
C_2H_6O	AR	Tianjin Xinbote Chemical Co.
$C_9H_{20}O_5Si$ (KH560)	97%	Aladdin
$(C_2H_5N)_n$, PEI	99%	Aladdin
TiO_2	99.8%	Aladdin
$(C_6H_{10}O_5)_n$	180 μm	Aladdin
Sand	10–15 nm	building materials factory
Macadam	10–15 mm	building materials factory

The instruments used during the experiment are listed in Table 5.

Table 5

Instruments used in the study

Fourier transform infrared spectrometer Nicolet iS50, Thermo Fisher Scientific
Scanning electron microscope – energy dispersive x-ray spectrometer EM-30AX, Coussem Company
Thermogravimetric differential scanning calorimeter, DMA242, NETZSCH
Universal testing machine for compression TYE-300D, Wuxi Jianyi Instrument Machinery Co., Ltd.
X-ray diffractometer, Axios, PANalytical B.V.
X-ray fluorescence spectrometer, S2 PUMA, Bruker Corporation

2.2. METHODS

Modified TiO_2. 20.0 g of titanium dioxide powder was dispersed in 100 cm^3 of ethanol solution within a 250 cm^3 three-necked flask. Silane coupling agent KH560 was added to the flask at three different concentrations (15%, 3 cm^3, 25%, 5 cm^3, 35%, 7 cm^3). The mixture underwent continuous stirring at 80 °C for 4 h. The resulting modified samples were designated as Ti15%, Ti25%, and Ti35% based on the KH560 concentration. The subsequent modification involved adding 25% (3 cm^3), 50% (10 cm^3), and 75% (15 cm^3) polyethyleneimine (PEI) solutions to the optimized Ti25% sample in the same reaction system. The reaction was maintained at 60 °C for 3 h under continuous stirring. The final modified samples were labeled as Ti25%-1, Ti25%-2, and Ti25%-3 according to PEI concentration. Following the reaction, the mixture was allowed to cool to ambient temperature and filtered under vacuum. The obtained precipitate was dried in an oven at 60 °C for 12 h to remove residual solvents. The dried product was ground into a fine powder using a mortar to ensure homogeneity. The specific reaction flow is shown in Figs. 2 and 3.

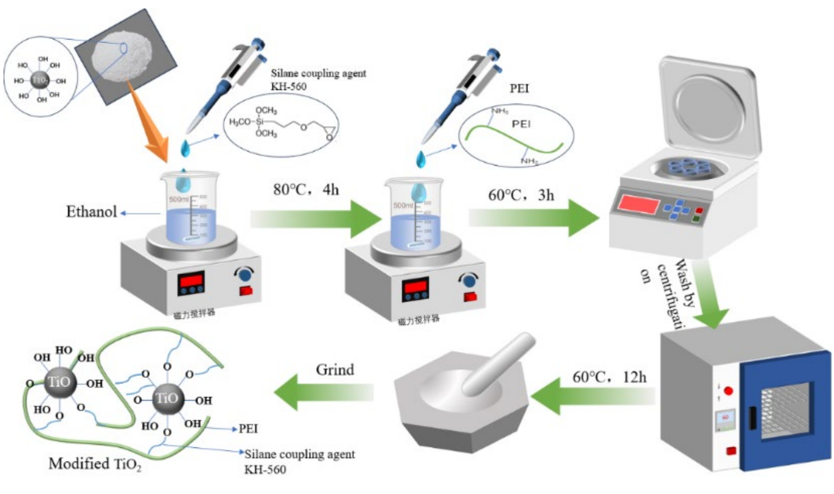

Fig. 2. Flow chart of TiO_2 modification

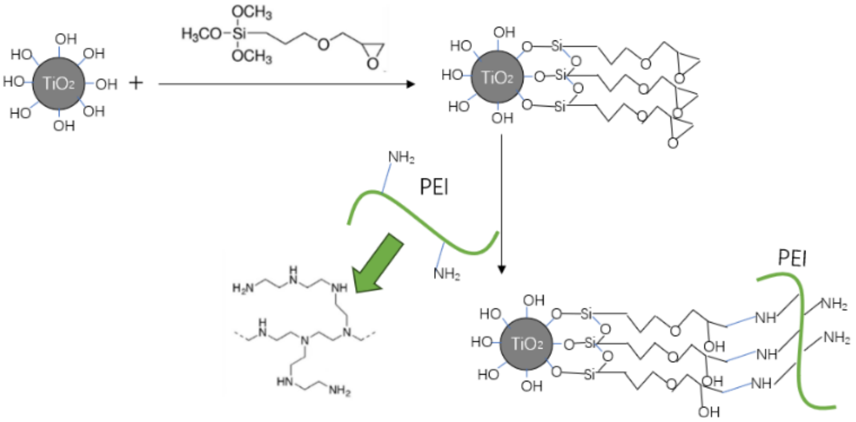

Fig. 3. Schematic diagram of the reaction of TiO_2 modification

Preparation of gold tailings-based no-fire bricks. The modified TiO_2 was added into the gelling materials (10 g of cement + 20 g of epoxy resin) in different proportions (1%, 2%, 3%). After adding 4 cm^3 of water, uniform stirring was conducted in a mixer for 1 min. Then sand (71 g), gold tailings (39 g), crushed stone (10 g), and cellulose (0.3 g) were put into the mixer and stirred for 5 min.

Table 6

Ingredients of curing specimens [g]

No.	Epoxy resin + cement	Crushed stone	Sand	Gold tailings	Modified TiO_2	Unmodified TiO_2	Cellulose
1	30	10	71	39	–	1.5 (1%)	0.3
2	30	10	71	39	–	3.0 (2%)	0.3
3	30	10	71	39	–	4.5 (3%)	0.3
4	30	10	71	39	1.5 (1%)	–	0.3
5	30	10	71	39	3.0 (2 %)	–	0.3
6	30	10	71	39	4.5 (3 %)	–	0.3

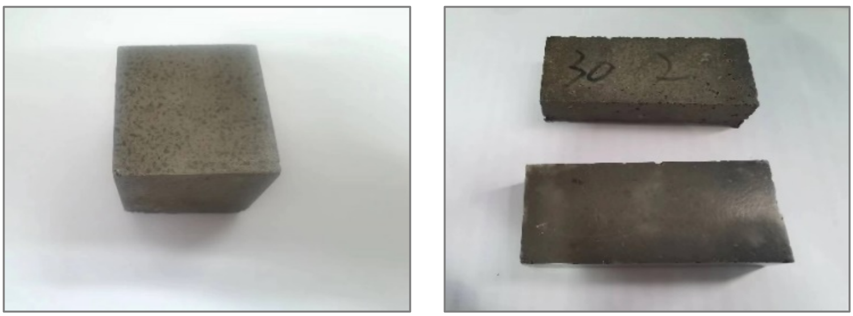

Fig. 4. Gold tailings-based no-fire bricks

The evenly mixed sample was poured into a cube mold with the size of 4 × 4 × 4 cm, and placed on a vibrating table for 2 min to remove air bubbles. The sample was demolded after curing at 25 °C for 24 h, and stored at room temperature for the rest of the time. Sample properties were examined on the 3rd and 28th day of curing. The specific ingredients are presented in Table 6. The bricks fabricated are shown in Fig. 4.

Water stability test. A comparative analysis was conducted on gold tailings-based no-fire bricks prepared under identical processing conditions. Three specimens cured under standardized environmental parameters (25±2° C, 101.3 kPa, 50±5% RH) for 28 days were systematically compared with three samples subjected to water immersion for 28 days. The water stability coefficient K_r and strength loss rate were calculated from:

$$K_r = \frac{q_{ut}}{q_{u0}}, \ \Delta q_t = \frac{q_{ut} - q_{u0}}{q_{u)}} \times 100\%$$

where Δq_t is the strength loss rate, %, q_{ut} the compressive strength of the brick samples cured by soaking in water on the 28th day, MPa, q_{u0} the compressive strength of the brick samples not cured by soaking in water on the 28th day, MPa.

Analytical testing. The Fourier infrared spectroscopy analysis was performed using an FTIR spectrometer to record the infrared spectra of TiO_2 samples before and after surface modification within the 4000–5000 cm^{-1} wavenumber range. This analysis aimed to identify characteristic functional groups and chemical bonding changes induced by the modification process. The microstructural observation utilized a scanning electron microscope equipped with energy-dispersive X-ray spectroscopy (SEM-EDS) to visualize the morphological features of the materials. Semi-quantitative elemental analysis was simultaneously conducted to determine the distribution and relative abundance of major elements.

The thermal behavior evaluation employed a synchronous thermal analyzer to perform thermogravimetric-differential scanning calorimetry (TG-DSC) under nitrogen atmosphere. Samples were heated from ambient temperature to 900 °C at a rate of 10 °C/min over 90 minutes, enabling the detection of physical transformations (e.g., phase transitions, melting) and chemical reactions (e.g., dehydration, decomposition). The mechanical property testing involved an universal testing machine operated at a loading rate of 1 kN/s to measure the compressive strength of the brick specimens. Three replicate tests were conducted, and the average value was reported to ensure statistical reliability.

3. RESULTS AND DISCUSSION

3.1. CHARACTERIZATION OF THE PROPERTIES OF MODIFIED TiO_2

3.1.1. COMPOSITION OF THE FUNCTIONAL GROUP

The FTIR spectra of the modified TiO_2 are shown in Fig. 5. They are almost identical to the spectra of the original sample. The peaks at 3262 cm^{-1} and 1640 cm^{-1} are due to the O–H stretching and bending vibration in the material, and the peaks at 3191 cm^{-1} and 1960 cm^{-1} are shifted and weakened after the modification. This spectral variation is primarily attributed to the chemical interaction between O–H on the TiO_2 surface and the silane coupling agent, which induced peak shifts and intensity attenuation at 2894 cm^{-1}.

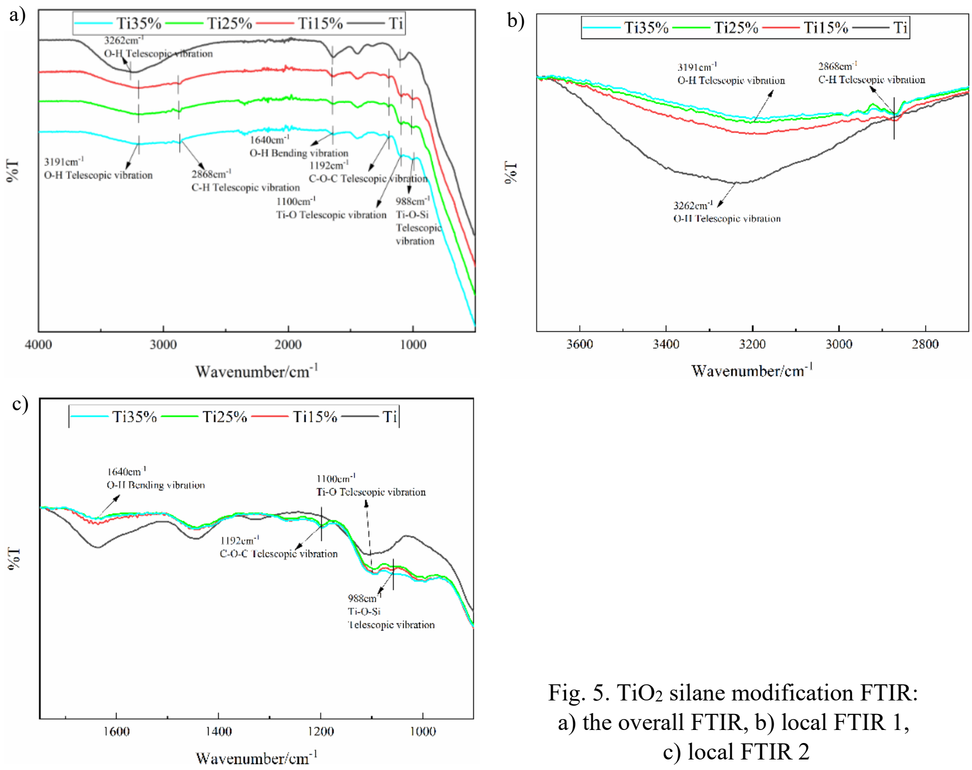

Fig. 5. TiO_2 silane modification FTIR: a) the overall FTIR, b) local FTIR 1, c) local FTIR 2

The new peak at 2894 cm^{-1} is mainly due to the stretching vibration of the C–H functional group produced by silane coupling agent [22]. The peak at 1100 cm^{-1} is due to the expansion and vibration of Ti–O in TiO_2, and the characteristic peak of Ti–O–Si appears at 988 cm^{-1} after modification, and leads to the weakening of Ti–O at 1100 cm^{-1}. Combined with the above analysis, the characterization of silane coupling agent KH560 did not change much after adding 25%, thus 25% silane coupling agent was chosen as the additive amount.

The FTIR spectra of the amine-based modified TiO_2 are shown in Fig. 6. The enhancement of modified TiO_2 at 3247 cm^{-1} is mainly due to channel water, O–H, N–H stretching vibrations. With the addition of polyethyleneimine, N–H undergoes a ring-opening reaction with the ether bond, which results in the weakening of C–O–C at 1192 cm^{-1}. With the increase of reaction time, the Ti–O and Ti–O–Si at 950–1100 cm^{-1} were shifted and strengthened to different degrees, which may be caused by the cross-linking of polyethyleneimine with silane coupling agent KH560, which leads to more substances grafted on the surface of TiO_2. The infrared analysis of the modified TiO_2 was performed by selecting 25% silane coupling agent and 75% polyethyleneimine.

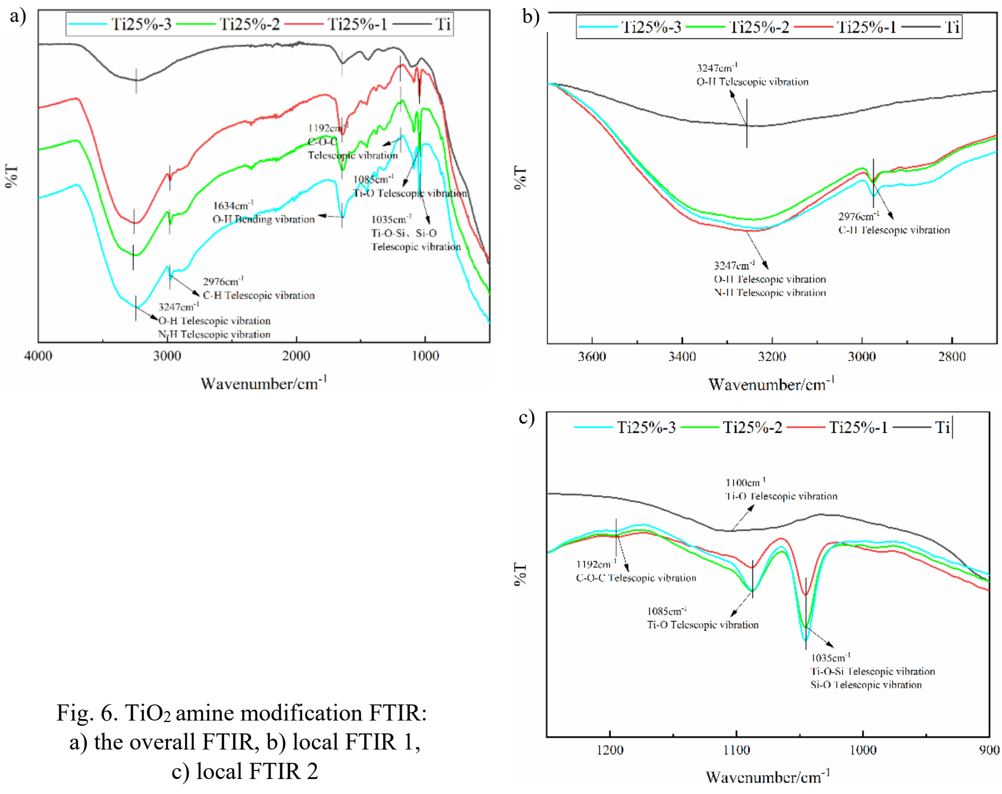

Fig. 6. TiO_2 amine modification FTIR: a) the overall FTIR, b) local FTIR 1, c) local FTIR 2

Through the infrared analysis in two parts of this subsection, after adding 25% of the silane coupling agent KH560 and 75% of polyethyleneimine, the increase or decrease and the intensity changes of the characteristic peaks such as O–H, C–H, C–O–C and Ti–O–Si indicate that the grafting effects of different amounts of the silane coupling agent and polyethyleneimine on the surface of TiO_2 are not exactly the same. Therefore, considering the economic aspect and the grafting effect, 25% of the silane coupling agent and 75% of polyethyleneimine are chosen as the modification of TiO_2 in this paper.

3.1.2. THERMAL DECOMPOSSITION

Thermal weight loss and crystalline phase transformation of TiO_2 samples before and after modification were tested by TG-DSC analysis of the samples with different modifications (Fig. 7).

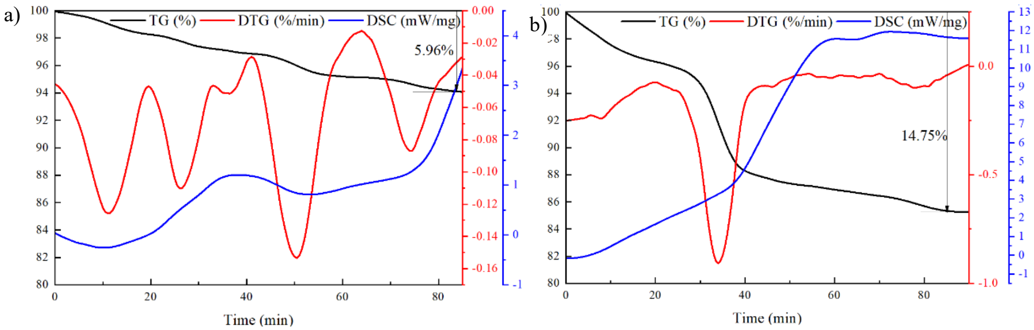

Fig. 7. TiO_2 TG-DSC plots before and after modification
a) unmodified TiO_2, b) modified TiO_2

The final heat weight loss of unmodified TiO_2 was 5.96%, and the weight loss peaks were haphazard, with more obvious weight loss rate peaks at multiple temperatures, mainly in the range of 200–550 °C, with the peak temperature at about 505 °C. Compared with the unmodified TiO_2, the final mass loss of TiO_2 modified with 25% silane coupling agent KH-560 and 75% polyethyleneimine (PEI) was 14.54%. An obvious thermal weight loss peak in the interval of 200–450 °C with the peak temperature at about 350 °C is mainly due to the thermal decomposition of polyethyleneimine. There is a more obvious weight loss peak at 750–850 °C, which is mainly due to the thermal decomposition of silane at 800 °C, resulting in the production of Si and H_2. The specific weight loss is shown in Table 7.

Table 7

Thermal weight loss data for TiO_2 [%]

Sample	Temperature range [°C]		Total
	200–450	750–850	
Unmodified TiO_2	1.62	0.50	5.96
Modified TiO_2	8.62	0.81	14.54

3.1.3. MICRO-MORPHOLOGICAL ANALYSIS

The SEM images of TiO_2 and modified TiO_2 products are shown in Fig. 8. Compared with the dispersed and finely ground TiO_2 product, the modified TiO_2 product formed a distinctive reticulated macromolecular structure. Due to the interlinking reaction between the KH560 and PEI, the molecular chains of the surface grafted product of the modified TiO_2 were crosslinked to form a more compact inter-particle arrangement, and the size of the particles increased significantly and ensured a certain pore volume. This is a favorable condition for the modified TiO_2 to promote the curing of the cementitious material. The particle size increased greatly and a certain pore volume was guaranteed; this provided favorable conditions for the modified TiO_2 to promote the curing of the cementitious material.

a)

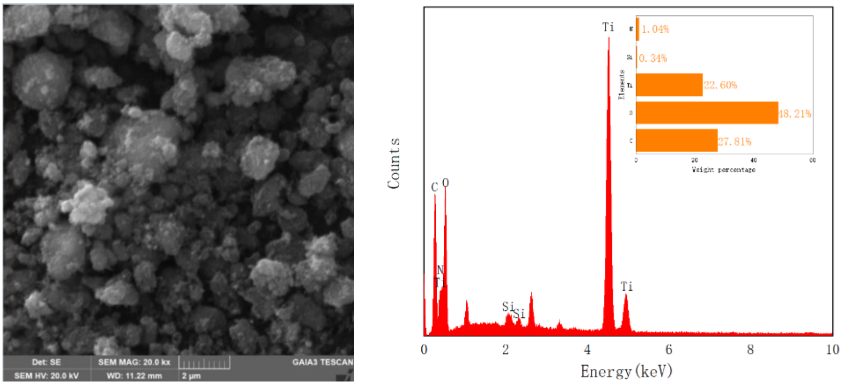

b)

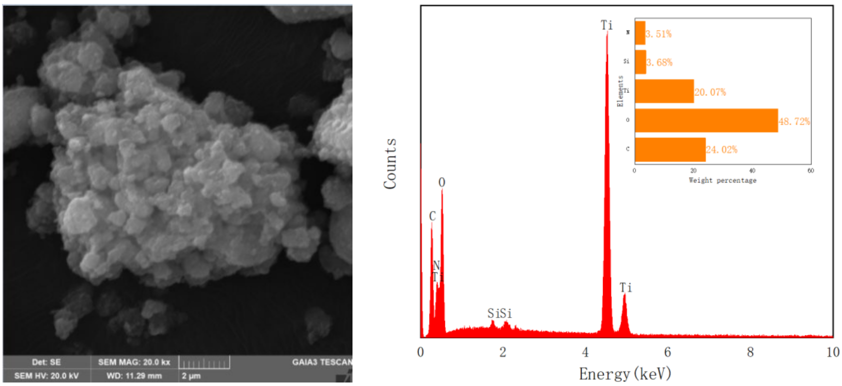

Fig. 8. SEM-EDS scans of TiO_2 before (a) and after (b) modification

The EDS images of unmodified TiO_2 and the modified TiO_2 are shown in Fig. 8. After the modification, Si content increased from 0.34% to 3.68%, and N content increased from 1.04% to 3.51%, mainly due to the Si in KH560, and N in PEI. The newly added Si and N are mainly distributed in the substances with irregular shapes on the surface of the modified TiO_2. From the morphological analysis, the Si and N elements also show a situation of uneven distribution. Through the content and distribution of the Si and N elements, it is proved that the modification of TiO_2 has been successful.

3.2. MECHANICAL PROPERTIES

3.2.1. EFFECT OF MODIFIED TiO_2 ON THE COMPRESSIVE STRENGTH

The compressive strength tests were conducted on the gold tailings-based non-fired bricks that have been cured for 3 and 28 days (Table 6). The results of the compressive strength test are shown in Fig. 9. When the modified TiO_2 was added at 2%, the best effect was achieved, and the compressive strengths on the 3rd day and 28th day were 49.5 and 79.6 MPa, respectively, which were 4.1 MPa (9.1%) and 9.8 MPa (14.0%) higher than those for the unmodified TiO_2, respectively. The compressive strength is mainly due to the three-dimensional spatial structure of the cured epoxy resin and the formation of crystalline and amorphous hydration products [23].

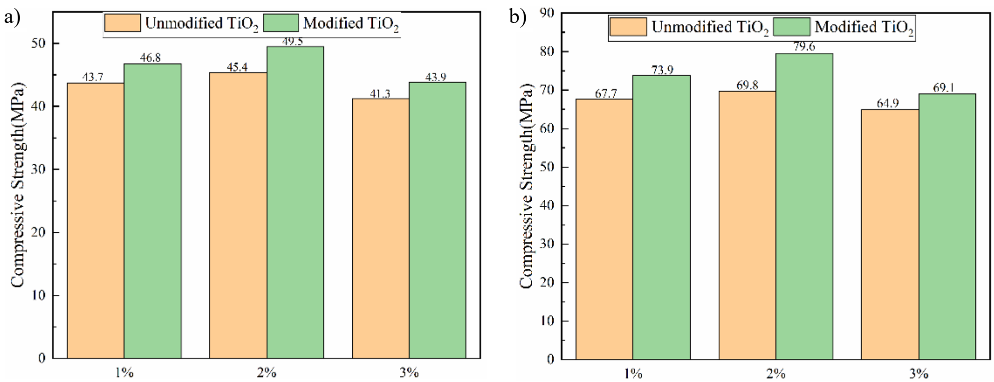

Fig. 9. Compressive strength of the gold tailings-based non-fired bricks versus the content of unmodified (a) and modified (b) TiO_2

On the one hand, the polymer on the surface of modified TiO_2 changes partly its physical and chemical characteristics, and because of the silanization of the surface, TiO_2 has Ti–O–Si chemical bonding, which can increase the surface's negative charges. Due to electrostatic repulsion, these negative charges can cause the TiO_2 to self-disperse in aqueous solution, boosting its dispersion performance in the no-fire brick slurry based on gold tailings. This can somewhat enhance the dispersion efficiency of TiO_2 in no-fire bricks made from gold tailings. On the other hand, the polyethyleneimine grafted on the surface of TiO_2 contains the active group $–NH_2$, which has active hydrogen atoms acting as nucleophiles and can undergo a ring-opening reaction with the epoxy groups with high reactivity in epoxy resin. Therefore, TiO_2 not only functions as a particulate filler but may also play a potential curing role for epoxy resin. Consequently, modified TiO_2 has a greater beneficial effect on the compressive strength of gold tailings-based no-fire bricks made than unmodified TiO_2.

3.2.2. EFFECT OF MODIFIED TiO_2 ON THE WATER STABILITY EXPERIMENTS

Water is a factor that has the greatest and the most long-term impact on the performance and service life of buildings. Long-term immersion in water will lead to erosion, causing damage to the internal structure of brick samples (such as cracks, voids, and the detachment of gelling materials). Therefore, the exploration of water stability is indispensable. In the experiment, under different conditions of routine maintenance and water immersion maintenance on the last day of the cured samples, the water stability data of the cured samples were tested. The parameters obtained in the experiments are shown in Table 8 and the compressive strength values are given in Fig. 10.

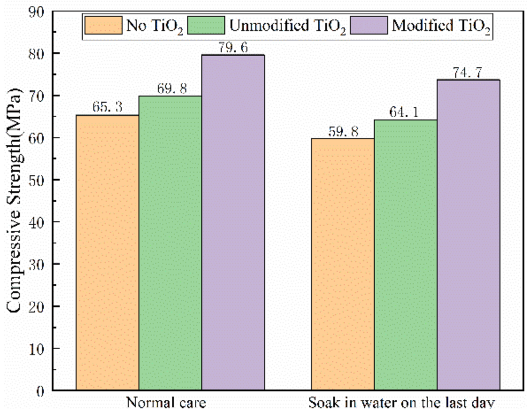

Fig. 10. Compressive strength under different nursing conditions: normal care: gold tailings-based no-fire bricks cured under standard conditions (ambient temperature, atmospheric pressure, and normal humidity) for 28 days

Table 8

Results of the water stability experiments

No.	Sample	Water stability coefficients	Strenght loss rate [%]
1	no TiO_2	0.91	9.95
2	2% unmodified TiO_2	0.92	8.17
3	2% modified TiO_2	0.94	6.15

Water stability coefficients vary only slightly and are all higher than the 0.85 required for water-resistant bricks. After being soaked on the last day, there was a certain degree of strength loss, with the loss rates being 9.95, 8.17, and 6.15% respectively. The absence of the strength increase indicates that the reaction of cement particles has been completed. With the addition of modified TiO_2, the curing effect of cement-epoxy resin is promoted, so the strength loss gradually decreases. However, since the film formed by epoxy resin plays a key role, the control of modified TiO_2 over strength loss is limited. It seems that the brick samples have good water stability, are less sensitive to water, and have good water resistance.

3.3. CHARACTERIZATION ANALYSIS

3.3.1. EFFECT OF MODIFIED TiO_2 ON THE FUNCTIONAL GROUP COMPOSITION

The FTIR spectra for co-addition of 2% modified and unmodified TiO_2, at 3rd day and 28th day of curing are shown in Fig. 11. The expansion and contraction vibration of the hydroxyl group (O–H) and amine group (N–H) is the absorption peak at 3397 cm^{-1}. The bonding water in the gelling material is represented by the bending vibration H–O–H at around 1605 cm^{-1}. The composition of epoxy resin A is the primary source of the asymmetric vibration of C–H at about 1503 cm^{-1}. According to the symmetric vibration of CO_3^{2-}, the absorption peak at 1445 cm^{-1} suggests that the material is somewhat carbonated.

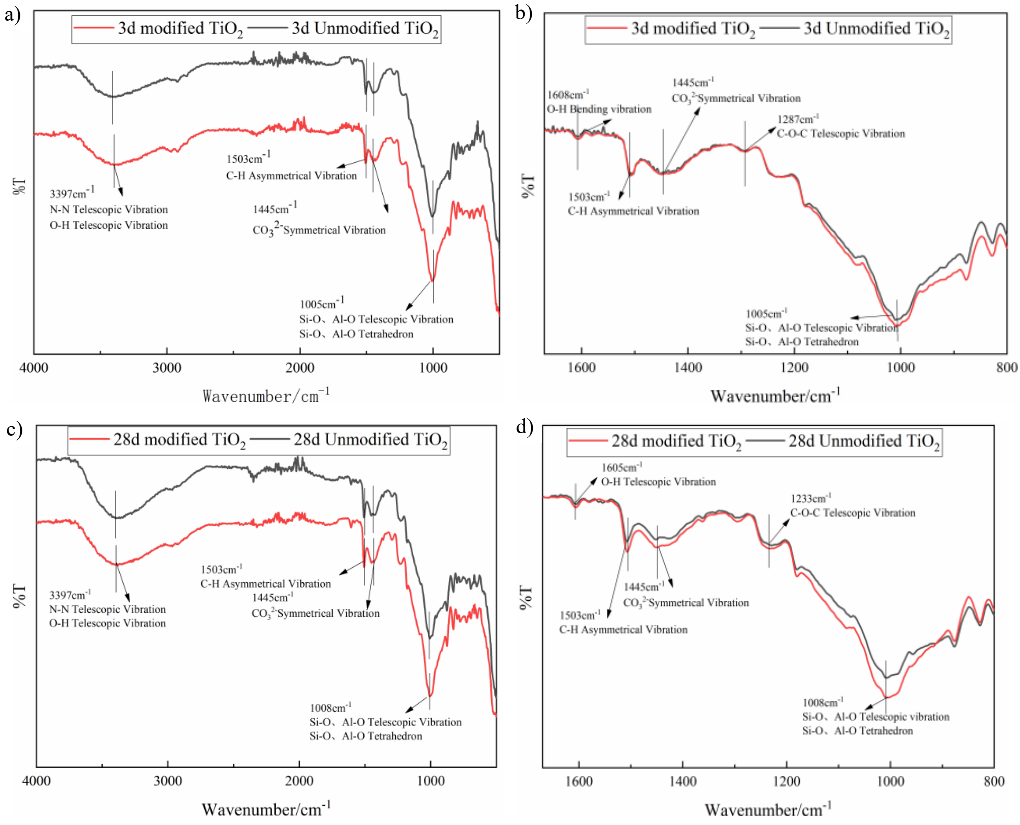

Fig. 11. FTIR spectra for different curing times: a) addition of TiO_2 3d cured brick samples, b) addition of TiO_2 3d cured brick samples (locally), c) addition of TiO_2 28d cured brick samples, d) addition of TiO_2 28d cured brick samples (locally)

The C–O–C telescopic vibration of absorption peaks includes 1233 cm^{-1}. The absorption peak at 966 cm^{-1} is the main characteristic peak of the gelling material, which is generated by the stretching vibration of the Si–O–T (T denotes Si or Al) structure, and the characteristic peak is shifted to the lower band, mainly due to the effect of Alate, so the gelling composition may be calcium silica-aluminate gel (C–A–S–H) or sodium silica-aluminate (N-A-S-H) [24–26].

At 28th day of curing, the addition of modified TiO_2 has greater characteristic peak transmittance at $CaCO_3$, calcium silica-aluminate gel (C–A–S–H)/sodium silica-aluminate (N–A–S–H) compared to the unmodified TiO_2 samples, suggesting that the modified TiO_2 has a certain promotion effect on the gelling material. And the N–H grafted on the surface of modified TiO_2 also has a certain promotion for the curing of epoxy resin, which leads to the increase of compressive strength.

3.3.2. EFFECT OF MODIFIED TiO_2 ON THE THERMAL CHARACTERISTICS

The TG-DSC spectra for co-addition of 2% modified and unmodified TiO_2 on the 3rd day and 28th day of the cured samples are shown in Fig. 12.

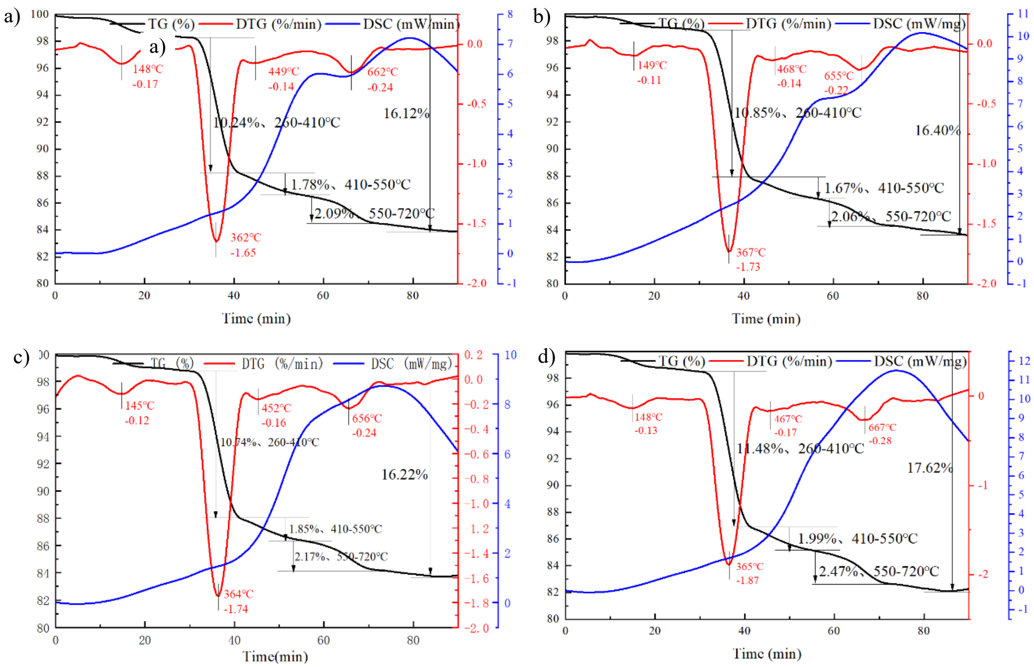

Fig. 12. TG-DSC plots for different curing times: a) unmodified TiO_2 3d cured brick samples, b) modified TiO_2 3d cured brick samples, c) unmodified TiO_2 28d cured brick samples, d) modified TiO_2 28d cured brick samples

The trend of the TG-DSC curves of the modified TiO_2 on the curing body was tested for 3d and 28d, and when the temperature increased to 900 °C, the mass loss rate of each specimen was 16.12, 16.40, 14.73, and 17.62%, and the mass loss mainly appeared below 450 °C, and the material's mass loss was more than 80%. The first peak of mass loss rate appeared at about 150 °C, mainly from the free water, adsorbed water and weakly bound water produced by the gradual decomposition of the gel in the gelling material. In the temperature range of 200–500 °C, the TG curve exhibited distinct mass loss, accompanied by the emergence of two mass-loss-rate peaks. These were primarily attributed to the decomposition of the epoxy resin at approximately 365 °C and the dehydrating decomposition of $Ca(OH)_2$ at around 460 °C. From 600 to 700 °C, the main reason is the loss of chemically bound water due to gel decomposition and the decomposition of $CaCO_3$ at ca. 600~700°C [27]. At 3 days, due to the rapid reaction of epoxy resin and the inhibition of the cement reaction process by the early-stage encapsulation, the mass loss between 410 °C and 720 °C was relatively low. At 28 days, the cement reaction process was able to proceed, and the losses of gel-bound water and the decomposition of $CaCO_3$ between 410 °C and 720 °C also gradually increased.

In Figure12, for the modified TiO_2 brick samples at 3 days, the mass losses between 410 °C and 720 °C were all less than those of the unmodified TiO_2 cured samples. This might be because the curing effect of $–NH_2$ on the surface of the modified TiO_2 promoted the reaction of epoxy resin and further inhibited the reaction of cement particles through encapsulation. At 28 days, the mass losses between 410 °C and 720 °C were all greater than those of the unmodified TiO_2 cured samples. As the reaction proceeded, the modified TiO_2 promoted the formation of C–S–H/C–A–H gels and $CaCO_3$. Consequently, the contents of gel-bound water and $CaCO_3$ increased, resulting in an increase in the DTG peak values at each stage and a relatively large mass loss for the modified TiO_2 cured samples.

3.4. MECHANISM OF THE EFFECT OF MODIFIED TiO_2 ON THE STRENGTH OF GOLD TAILINGS-BASED NON-FIRED BRICKS

On the one hand, after the surface modification of TiO_2, its physical and chemical properties changed. In the Ti–O–Si bond, since the electronegativity of Si is greater than that of Ti, the electron cloud will be more inclined to the O–Si side, increasing the electron cloud density around O and thus making it carry more negative charges. The Ti–O–Si chemical bonds abundant on the surface make the surface of TiO_2 carry more negative charges. Due to the principle *that poles repel each other*, it is more conducive to the dispersion of TiO_2. On the other hand, the particle size of TiO_2 was between 5 and 10 nm before modification, and between 8–16 nm after modification. Due to the increase in particle size, as well as the changes in specific surface area and surface energy, the agglomeration performance of the nanomaterials will also be weakened to a certain extent. Therefore, the modified TiO_2 has better dispersion in gold tailings-based no-fire bricks and can give fuller play to the “nucleation effect” of TiO_2, enabling it to enhance the curing effect of the epoxy resin-cement gel. Therefore, modified TiO_2 can make the curing more dense and improve its mechanical properties. At the same time, its strong water absorption and hydrophilicity can easily adsorb nearby cations (Ca^{2+}, Al^{3+}, etc.), prompting the cement to react sufficiently and increasing the gel generation of $CaCO_3$, C–A–S–H, C–S–H, etc., as shown in Fig. 13.

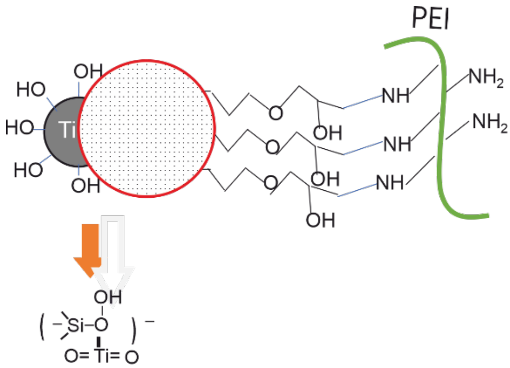

Fig. 13. TiO_2 charged pattern

The nucleation effect of modified TiO_2 is more prominent, which can be primarily attributed to the surface-grafted N-H groups reacting with the ether bonds in the epoxy resin matrix. This interaction accelerates the solidification process of the epoxy resin, forming an initial interfacial layer structure. The subsequent formation of C–A–S–H/C–S–H gels generates a secondary network structure. The cross-linking between these two layers of gelling materials during the curing process leads to rapid strength development and enhancement. During the formation of the two-layer gelling materials, they cross-link with each other. This cross-linking enables the rapid formation and improvement of strength. The specific mechanism is shown in Fig. 14.

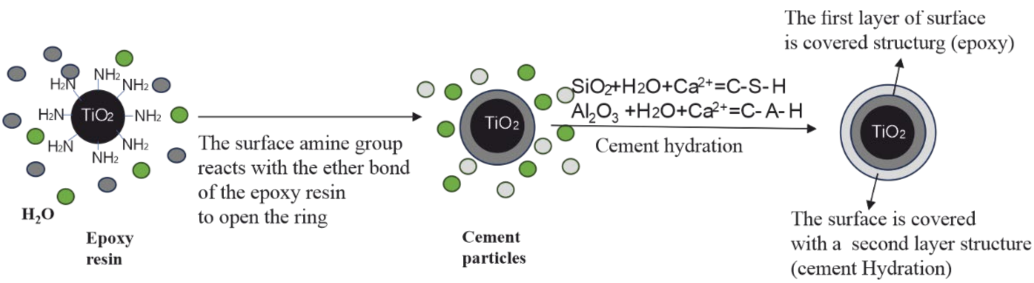

Fig. 14. Nucleation effect of modified TiO_2

4. CONCLUSIONS

The preparation of modified TiO_2 and its effect on the strength of gold tailings--based no-fire bricks were investigated. This study mainly focused on two aspects: the preparation of modified TiO_2 and strength testing to evaluate its effect on gold tailings-based no-fire bricks. The main conclusions are as follows:

- According to FTIR, TG-DSC, SEM-EDS analyses, the successful modification of the TiO_2 surface was proved. The grafting rate was more excellent when modification with 25% silane coupling agent and 75% polyethyleneimine was applied. The Si content increased significantly from 0.34% to 3.68%, while the N content increased from 1.04% to 3.51% in the modified sample compared to the unmodified counterpart.
- When 2% modified TiO_2 was added, the compressive strengths of the samples reached 49.5 and 79.6 MPa at 3 days and 28 days of curing, respectively. Moreover, the compressive strength was improved by 9.1 and 14.0% compared with the samples without the addition of modified TiO_2 at the corresponding curing times. The compressive strength is mainly formed by the three-dimensional spatial structure of the cured epoxy resin and the formation of crystalline and amorphous hydration products by the hydration reaction.
- FTIR, TG-DSC, and XRD analyses of gold tailings-based no-fire bricks indicate that the modification process enhances the dispersion uniformity of TiO_2 within the matrix, and promotes the hydration reaction of cementitious materials in the bricks. And the surface amine group has a latent curing effect on epoxy resin. Thus, the hardened body structure of gold tailings-based no-fire bricks is denser, which achieves the effect of enhancing strength. Compared with traditional brick-making, the method of applying modified TiO_2 as a reinforcing agent to gold tailings-based no-fire bricks can improve the insufficient curing performance of conventional cementitious materials to a certain extent, reduce the economic cost and environmental pollution caused by pressure sintering in the brick-making process, and can also alleviate the problem of large-scale accumulation of gold tailings. However, there are still shortcomings in this experiment:

– A shortcoming, the grafting rate of silane coupling agent with polyethyleneimine on the surface of TiO_2 nanoparticles is not particularly desirable, and the large addition of the modifier will increase the economic cost to some extent.

– On the other hand, the gold tailings-based no-fire bricks are affected by the physical and chemical properties of the gold tailings, and the amount of gold tailings added is not particularly satisfactory.

ACKNOWLEDGEMENTS

This work was supported by the Basic Scientific Research Operating Expenses Project of Universities (No. 2024RCTD002).

REFERENCES

[1] MACÍAS-MACÍAS K.Y., CENICEROS-GÓMEZ A.E., GUTIÉRREZ-RUIZ M.E., GONZÁLEZ-CHÁVEZ J.L., MARTÍNEZ-JARDINES L.G., *Extraction and recovery of the strategic element gallium from an iron mine tailing*, J. Environ. Chem. Eng., 2019, 7, 102964. DOI: 10.1016/j.jece.2019.102964.

[2] YI L., MI H., WU Q., XIA J., ZHANG B., *Present situation of comprehensive utilization of tailings resources in China*, Conserv. Util. Miner. Res., 2020, 40 (3), 79–84. DOI: 10.13779/j.cnki.issn1001-0076.2020.03.013.

[3] QAIDI S.M.A., MOHAMMED A.S., AHMED H.U., FARAJ R.H., EMAD W., TAYEH B.A., ALTHOEY F., ZAID O., SOR N.H., *Rubberized geopolymer composites: A comprehensive review*, Ceram. Int., 2022, 48, 24234–24259. DOI: 10.1016/j.ceramint.2022.06.123.

[4] MA L., LIU J., *Comprehensive utilization analysis of tailings*, Sci. J. Technol., 2022, 4 (8), 1648. DOI: 10.54691/sjt.v4i8.1648.

[5] CHEN W., YIN S., CHEN X., WANG L., ZHANG M., *Study on comprehensive utilization of tailings by using bioleaching and microbial-cementation*, Case Stud. Constr. Mater., 2023, 18, e02190. DOI: 10.1016/j.cscm.2023.e02190.

[6] CHEN W., YIN S., ZHOU G., LI Z., SONG Q., *Copper recovery from tailings through bioleaching and further application of bioleached tailings residue: comprehensive utilization of tailings*, J. Clean. Prod., 2022, 332, 130129. DOI: 10.1016/j.jclepro.

[7] WANG P., LI J., HU Y., CHENG H., *Solidification and stabilization of Pb-Zn mine tailing with municipal solid waste incineration fly ash and ground granulated blast-furnace slag for unfired brick fabrication*, Environ. Pollut., 2023, 321, 121135. DOI: 10.1016/j.envpol.

[8] ZHOU X., ZHANG Z., YANG H., *Stabilization/solidification mechanisms of tin tailings and fuming slag-based geopolymers for different heavy metals*, FESE, 2024, 18 (5), 43–55. DOI: 10.1007/s11783-024-1816-3.

[9] WEI Z., ZHAO J., WANG W., YANG Y., HOU Z., *Utilizing gold mine tailings to produce sintered bricks*, Constr. Build. Mater., 2021, 282 (4), 122655. DOI: 10.1016/j.conbuildmat.2021.122655.

[10] IKOTUN J.O., ADEYEYE R.A., OTIENO M., *Experimental investigation on the effect of gold tailings as a partial replacement for sand in concrete*, Sustainability, 2024, 16 (17), 7762. DOI: 10.3390/su16177762.

[11] URIBE L., MORAGA C., RIVAS F., *Using gold-silver tailings on the elaboration of ceramic foams*, Sustain. Metall., 2021, 7, 364–376. DOI: 10.1007/s40831-021-00365-z.

[12] XI L., NI Y., CAI P., *Application of the dual indexes of sand content and fineness modulus in the delineation of a marine sand mining area for backfilling purposes in Guangdong and the estimation of its resource quantity*, Mar. Geol. Front., 2025, 41 (01), 93–101. DOI: 10.16028/j.1009-2722.2023.280.

[13] ARULMOZHI S., ARASI S.E., *Size controlled synthesis of gadolinium doped titanium dioxide nanoparticles by low-temperature hydrothermal method towards effective photovoltaic application*, Mater. Today Proc., 2020, 50 (7), 2756–2759. DOI: 10.1016/j.matpr.2020.08.456.

[14] CHEN Q., TONG R., XIANJIE X., *Ultrafine ZnO quantum dot-modified TiO_2 composite photocatalysts: the role of the quantum size effect in heterojunction-enhanced photocatalytic hydrogen evolution*, Catal. Sci. Technol., 2018, 8, 1296–1303. DOI: 10.1039/C7CY02310C.

[15] HSU C.-Y., MAHMOUD Z.H., ABDULLAEV S., ALI F.K., NAEEM Y.A., MIZHER R.M., KARIM M.M., *Nano titanium oxide (nano-TiO_2): a review of synthesis methods, properties, and applications*, Case Stud. Chem. Environ. Eng., 2024, 9, 100626. DOI: 10.1016/j.cscee.2024.100626.

[16] ROY J., *The synthesis and applications of TiO_2 nanoparticles derived from phytochemical sources*, J. Ind. Eng. Chem., 2021, 106, 1–19. DOI: 10.1016/j.jiec.2021.10.024.

[17] YANG F., XIE J., WANG W., WANG W., WANG Z., *The role of nano-TiO_2 on the mechanical properties and hydration behavior of C2S, C3S and C4A3S*, Constr. Build. Mater., 2023, 388, 131558. DOI: 10.1016/j.conbuildmat.2023.131558.

[18] AMOR F., BAUDYS M., RACOVA Z., SCHEINHERROVÁ L., INGRIŠOVÁ L., HÁJEK P., *Contribution of TiO_2 and ZnO nanoparticles to the hydration of Portland cement and photocatalytic properties of high-performance concrete*, Case Stud. Constr. Mater., 2022, 16, e00965. DOI: 10.1016/j.cscm.2022.e00965.

[19] SHAFAEI D., YANG S., BERLOUIS L., MINTO J., *Multiscale pore structure analysis of nano titanium dioxide cement mortar composite*, Elsevier, 2020, 22, 100779. DOI: 10.1016/j.mtcomm.2019.100779.

[20] AHMED H.U., MAHMOOD L.J., MUHAMMAD M.A., FARAJ R.H., QAIDI S., SOR N.H., MOHAMMED A.S., MOHAMMED A.A., *Geopolymer concrete as a cleaner construction material: An overview on materials and structural performances*, Clean Mater., 2022, 5, 100111. DOI: 10.1016/j.clema.2022.100111.
[21] MALEKI A., HAJIZADEH Z., FIROUZI-HAJI R., *Eco-friendly functionalization of magnetic halloysite nanotube with so3h for synthesis of dihydropyrimidinones*, Micropor. Mesopor. Mater., 2018, 259, 46–53. DOI: 10.1016/j.micromeso.2017.09.034.
[22] DENG Z., ZHOU W., YUE H., GUO X., *Study on the hydration mechanism of a hardened slag-based plugging agent activated by alkalis*, Constr. Build. Mater., 2019, 203 (Apr. 10), 343–355. DOI: 10.1016 /j.conbuildmat.2019.01.015.
[23] ZHAO S., XIA M., YU L., HUANG X., LI D., *Optimization for the preparation of composite geopolymer using response surface methodology and its application in lead-zinc tailings solidification*, Constr. Build. Mater., 2021, 266, 120969. DOI: 10.1016/j.conbuildmat.2020.120969.
[24] XU X., QI C., ARETXABALETA X.M., CHUNDI M., DINO S., HEGOI M., *The initial stages of cement hydration at the molecular level*, Nat. Commun., 2024, 15, 2731. DOI: 10.1038/s41467-024-46962-w.
[25] LEI J., LAW W.W., YANG E., *Effect of calcium hydroxide on the alkali-silica reaction of alkali-activated slag mortars activated by sodium hydroxide*, Constr. Build. Mater., 2021, 272, 121868. DOI: 10.1016/j.conbuildmat.2020.121868.
[26] GAO W., NI W., ZHANG Y., LI Y., SHI T., LI Z., *Investigation into the semi-dynamic leaching characteristics of arsenic and antimony from solidified/stabilized tailings using metallurgical slag-based binders*, J. Hazard. Mater., 2020, 381, 120992. DOI: 10.1016/j.jhazmat.2019.120992.
[27] ZOU S., SUN Z., LU Z., YANG H., LI H., FAN S., DENG X., YANG J., *Fresh and hardened properties of cement paste under the synergistic influence of polycarboxylate superplasticizer and anionic polyacrylamide*, Case Stud. Constr. Mater., 2024, 21, e03895. DOI: 10.1016/j.cscm.2024.e03895.